Recent Advances on Pseudodynamic Hybrid Simulation of Masonry Structures

G. Abbiati[1*], G. Miraglia[2], B. Stojadinovic[1]

[1]*Department of Civil, Environmental and Geomatic Engineering (D-BAUG), IBK, ETH Zurich, Switzerland*

[2]*Department of Structural, Geotechnical and Building Engineering (DISEG), Polytechnic of Turin, Italy*

ABSTRACT

Hybrid Simulation has been introduced to simulate the seismic response of civil structures. The hybrid model of the emulated system combines numerical and physical subdomains and its dynamic response to a realistic excitation is simulated using a numerical time-stepping response history analysis. In the current practice, lumped parameters structural topologies such as shear type frames or inverted pendulum characterize the physical subdomain and the design of the testing setup is straightforward. Although hybrid simulation has been extensively exploited for testing concrete and steel structures, in the authors' knowledge, there is still a paucity of scientific publications devoted to masonry applications. This is in contrast to the inherent uncertainty carried by masonry failure mechanisms, which hinders any attempt of implementing predictive numerical models. From this perspective, this paper summarizes our recent research achievements aimed at extending hybrid simulation to distributed parameter specimens, such as masonry walls, using the minimum number of actuators. The great potential of reduction bases in driving the substructuring process has been shown in a previous work and here is enhanced to floating physical subdomains.

Keywords: *hybrid simulation, substructuring, distributed parameter systems, masonry structure retrofitting.*

1 INTRODUCTION

Hybrid Simulation (HS), which is also known as Hardware-in-the-Loop (HiL) testing, has been introduced in the seventies to simulate the seismic response of civil structures, [1], [2]. The hybrid model of the emulated system combines numerical and physical subdomains (NS and PS) and its dynamic response to a realistic excitation is simulated using a numerical time-stepping response history analysis. A computer-controlled system applies displacements to the PS using hydraulic/electric servo-actuators and corresponding restoring forces are measured from these degrees of freedom (DOFs) using load cells and fed back to the hybrid model. Then the equation of motion is solved at the next time step. When the response of the PS does not depend on the rate of loading, a pseudodynamic (PSD-) HS can be performed at an extended time scale, typically in the broad range of 50-200 times slower than the actual earthquake, requiring inertia and damping forces to be modelled numerically. Real-time (RT-) HS is a special case of PSD-HS when a unit time scale is applied. Lack of reliable mathematical models or strongly nonlinear responses justify the experimental substructuring of a system subcomponent, i.e. the PS, while well-known subparts are instantiated in a numerical simulation software, namely computational environment, as NS. Although HS has been extensively exploited for testing concrete and steel structures, in the authors' knowledge, there is still a paucity of scientific publications devoted to masonry applications. This is in contrast to the inherent uncertainty carried by masonry failure mechanisms, which hinders any attempt of implementing predictive numerical models. Paquette and Bruneau, [3], [4], used PSD-HS to understand the flexible-floor/rigid-unreinforced-wall interaction during earthquake and the

* abbiati@ibk.baug.ethz.ch

effectiveness of the use of fiberglass strips for retrofitting purposes. Pinto and co-workers, [5], performed PSD-HS of different historical constructions subjected to earthquake loading. The extreme sensitivity of friction-based analytic models with respect to assumed friction coefficients motivated Buonopane and White to simulate the seismic response of a frame infilled with masonry by means of PSD-HS, [6]. Along the same line, [7], assessed the seismic performance of a multi-story infilled frame through PSD-HS and observed a strong correlation between wall damage and hysteretic energy dissipation.

In our opinion, the limited application of HS to masonry structures must be ascribed to the difficult encountered in the substructuring process when distributed mass, stiffness and boundaries are involved. If lumped parameters structural topologies such as shear type frames or inverted pendulum characterize the PS, the design of the testing setup is straightforward: subdomain boundaries are punctual and a few actuators handle the totality of physical DOFs. Conversely, a few attempts to handle distributed parameter PSs exists. Hashemi and co-workers, [8], proposed a methodology for testing multistory buildings with a reduced number of actuators exploiting subdomain overlapping. Additional strain gauges provided estimates of member internal forces in experimental columns, which were used to impose rotations to structural nodes. Along the same line, Bursi and co-workers, [9], introduced the concept of reduction basis in the design of the experimental setup. In detail, they developed a testing design procedure based on Principal Component Analysis (PCA) that allows for optimizing number and position of actuators when distributed parameter specimens are involved. As a result, they successfully performed PDT- and RT-HSs to assess the seismic performance of a flexible piping network.

With reference to the sole PDT method, the present paper generalizes the procedure of Bursi and co-workers to floating PSs. In this particular case, connection to the NS provides the only constraints to the PS, whose dynamic response is a superposition of rigid body and deformation modes. It is noteworthy that in the static case, rigid body modes do not generate restoring forces since they form the kernel of the stiffness matrix. Accordingly, the testing setup is optimized to impose the pure deformation component of the PS response to the tested specimen, which is fixed to the reaction frame in a statically determined configuration. The "Regina Montis Regalis" Basilica of Vicoforte is selected as masonry proof-of-concept case study for the numerical validation. A linear Finite Element (FE) model of the drum-dome system is implemented and a portion of the drum is supposed to be substructured in the laboratory as PS. To this end, a FE simulation software is coded in the Matlab environment in order to support future experimental implementations on real-time computers.

2 DESCRIPTION OF THE VICOFORTE CASE STUDY

In order to demonstrate the effectiveness of the developed approach, the 25 x 35 m elliptical dome-drum system of the “Regina Montis Regalis” Basilica of Vicoforte is selected as reference case study. Such structural system suffered over the years from significant structural problems, partly due to settlements of the building induced progressively by newly built masses. The tie-bars system consisting of three iron rings, which was embedded during the construction of the dome in 1734, testifies the critical structural health condition of the drum-dome system since the early stages of its construction. The continuity of such strengthening was tested by using an Impact Echo Scanner in 2004, [10]. As shown in Fig. 1, a widespread system of cracks encompasses various zones of the structure. The most important cracks cross the drum up to dome oval openings. Then, meridional cracks propagate downward from the buttresses beneath the drum evidencing and confining load paths converging to main base pillars, [11]. In order to limit the crack growth, a strengthening intervention was accomplished in 1987, when 56 active slightly tensioned steel 32 mm diameter tie-bars, for a total cross-section of 3200 mm^2, were placed within holes drilled in the masonry at the top of the drum along 14 tangents around the perimeter. Fig. 2 offers a schematic view of the strengthening system.

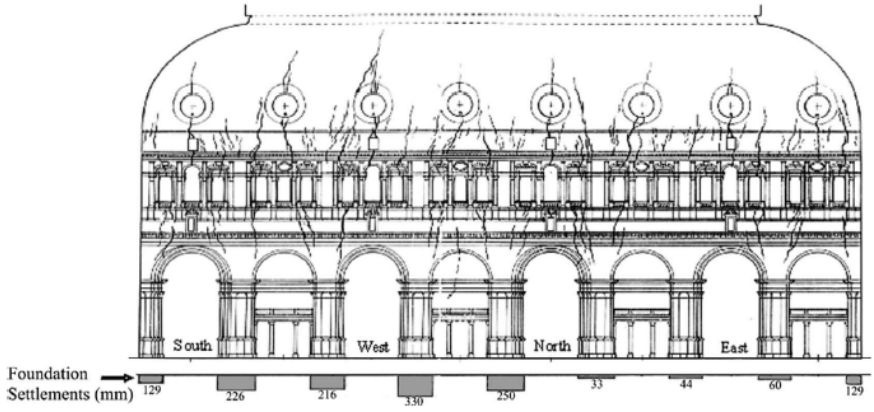

Figure 1 - Schematic of crack patterns and foundation settlements.

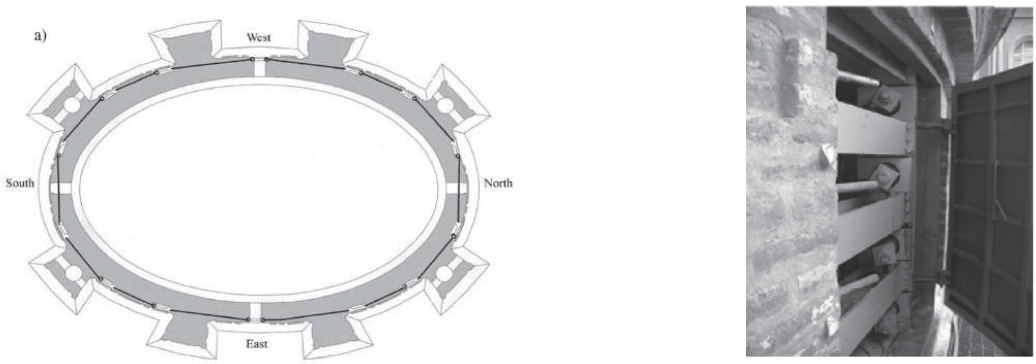

a b

Figure 2 - Strengthening system based on slightly tensioned bars realized in 1987.

As shown fin Fig. 2, steel frames were interposed between each pair of bar segments so as to seam the drum structure. In 1997, bars were re-tensioned to compensate stress losses, [12]. In general, a rigorous model-based evaluation of the effectiveness of masonry strengthening interventions is very often impracticable. The limited knowledge on force redistribution due to contact, friction and cracks motivated the authors in exploring the application HS to masonry structures.

3 FINITE ELEMENT MODEL OF THE DRUM-DOME SYSTEM

An accurate FE model of the Basilica of Vicoforte has been created over the last decade, also thanks to an experimental testing campaigns and successive FE calibrations, based on both static and dynamic monitoring data, [13], [14]. On this basis, a 1231-node and 1230-element FE model of sole the dome-system was derived to support the validation of the proposed procedure. The decision of manually code the FE model in the Matlab environment was dictated by two strict requirements: i) retrieving system matrices; ii) performing reasonably long time history analyses with reduced memory storage. Such functions are typically not provided by commercial software. Moreover, developed elements can be easily adapted to a real-time computational environment for the purpose of conducting HS. The geometry of the dome approximates an ellipsoidal shape of axes of 37.15, 24.80 and 40.00 m, in X, Y and Z direction, respectively, and it is discretized in 82 sectors of 15 elements along the meridian direction. A uniform average thickness of 1.24 m is considered according to recent geo-radar scans. The size of the base ring elements approaches the dimension of the 1.20 m width, 2.00 m depth steel frames, which are represented by plate element of 0.015 m equivalent thickness. A 4-node membrane element was used for all rings, except for the last level where 3-node membrane elements were necessary. A set of multi-axial springs support the dome so as to simulate the interaction with the remainder of the structure. The stiffnesses along the X, Y and Z directions

were evaluated at approximately 3.4e7 N/m, 3.4e7 N/m and 3.8e7 N/m, respectively. Fig. 3 shows the implemented FE model with PS and NS partitioning highlighted.

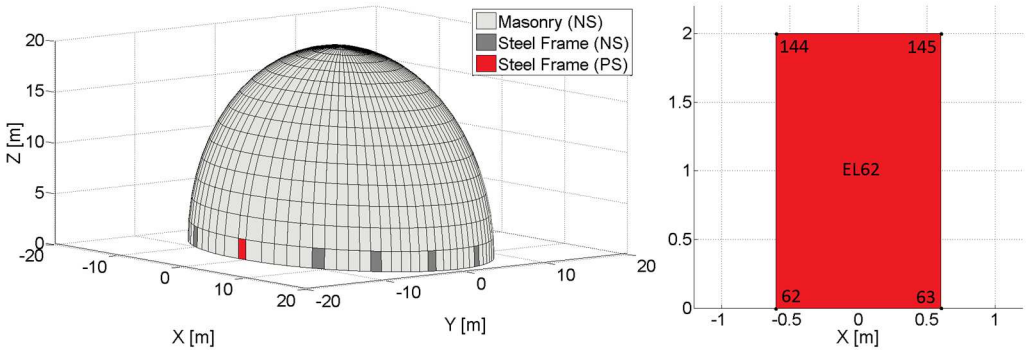

Figure 3 - Finite elements substructured mesh of the drum-dome system.

As can be appreciated from Figure 3, a single steel frame is supposed to be substructured in the laboratory as PS. For the sake of clarity, system DOFs are indicated with the number of the corresponding node and a displacement field component. For example, DOF 144-X corresponds to the X displacement of node 144. Table 1 summarizes the parameters of all materials, which are assumed to be linear elastic.

Table 1: Material parameters

Element	***E* [GPa]**	***υ***	***ρ* [kg/m^3]**
Masonry	5.9	0.35	1800
Steel	210	0.30	7800

Table 2 summarizes the first five eigenfrequencies of the structure while Fig. 4 depicts the deformed shapes of the first two modes.

Table 2: Eigenfrequencies of the drum-dome system

Mode	**Frequency [Hz]**
1	2,18
2	2,90
3	4,30
4	4,85
5	5,00

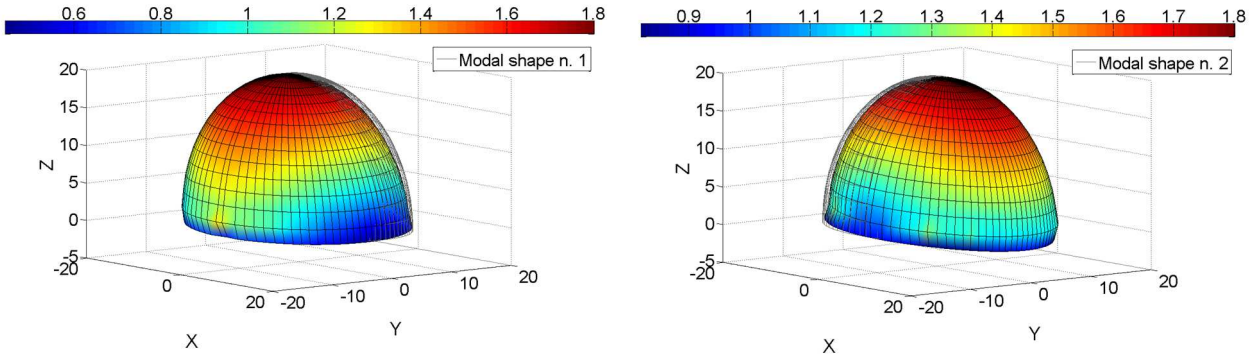

a *b*

Figure 4 - Deformed shape of the drum-dome system of: a) Mode 1 at 2.18 Hz; and b) Mode 2 at 2.90 Hz.

The implementation of each single element as well as the overall model were validated with respect to solutions provided by the ANSYS FE code, [15].

4 TEST DESIGN PROCEDURE

4.1 Substructuring framework

The substructuring framework is introduced for the selected drum-dome system subjected to a seismic excitation, whose equation of motion reads,

$$\mathbf{M}\ddot{\mathbf{u}} + \mathbf{C}\dot{\mathbf{u}} + \mathbf{K}\mathbf{u} = -\mathbf{M}\mathbf{t}\ddot{u}_g \tag{1}$$

where, **M**, **C**, and **K** are mass, damping and stiffness matrices, respectively and **t** is a Boolean vector that project the seismic acceleration on the system DOFs. In line with the PDT-HS method, which splits the emulated system into PS and NS, Eq. (1) turns into,

$$\begin{cases} \left(\mathbf{M}^N + \mathbf{M}^P\right)\ddot{\mathbf{u}} + \left(\mathbf{C}^N + \mathbf{C}^P\right)\dot{\mathbf{u}} + \mathbf{K}^N\mathbf{u} = -\left(\mathbf{M}^N + \mathbf{M}^P\right)\mathbf{t}\ddot{u}_g - \mathbf{r}^P \\ \mathbf{r}^P = \mathbf{K}^P\mathbf{u} \end{cases} \tag{2}$$

In detail, superscript P and N refer to NS and PS and, $\mathbf{r}^P$ condenses the experimental response of the latter. Along the same criterion, the set of system DOFs can be partitioned on three disjoint subsets. One subset is restricted to interface DOFs connecting NS and PS while the other two gather pure numerical and physical DOFs,

$$\mathbf{u} = \begin{bmatrix} \mathbf{u}^N \\ \mathbf{u}^I \\ \mathbf{u}^P \end{bmatrix} \tag{3}$$

For brevity, the following simplified notation holds: N-DOFs, P-DOFs and I-DOFs, for pure numerical, pure physical and interface DOF, respectively. In this context, all matrices and vectors of Eq. (2) and (3) must be intended as expanded to the three DOF subsets thereof. For the sake of clarity, the experimental displacement vector $\mathbf{u}^E$ is defined as,

$$\mathbf{u}^E = \begin{bmatrix} \mathbf{u}^I \\ \mathbf{u}^P \end{bmatrix} \tag{4}$$

It must be emphasized that the displacement response of the PS spans rigid body modes when the only constraint is provided by the connection to the NS. Rigid rotations and translations define the kernel of the PS stiffness matrix,

$$\mathbf{R}^P = \ker\left(\mathbf{K}^P\right) \tag{5}$$

In the PDT practice, the specimen is constrained to a reaction frame in a statically determined configuration and rigid body components are removed from the PS response so as to apply a pure deformation field to the specimen. This is of paramount importance for calculating all reaction forces, which are part of the restoring force vector $\mathbf{r}^P$ and cannot be measured directly from actuator load

cells. Both the experimental displacement vector $\mathbf{u}^E$ and the rigid body mode matrix $\mathbf{R}^P$ are partitioned according to retained or constrained experimental DOFs. At each time step k of the simulation, the rigid body response vector $\boldsymbol{\lambda}$ is calculated and purged from the PS response,

$$\begin{bmatrix} \mathbf{R}^{P,r} \\ \mathbf{R}^{P,c} \end{bmatrix} \boldsymbol{\lambda}_k + \begin{bmatrix} \mathbf{u}_k^{E,r} \\ \mathbf{u}_k^{E,c} \end{bmatrix} = \begin{bmatrix} \overline{\mathbf{u}}_k^{E,r} \\ \mathbf{0} \end{bmatrix} \tag{6}$$

where superscript r and c stand for retained and constrained DOFs and,

$$\boldsymbol{\lambda}_k = -\left(\mathbf{R}^{P,c}\right)^{-1} \mathbf{u}_k^{E,c} \tag{7}$$

As a result, the pure deformation component $\overline{\mathbf{u}}^{E,r}$ of the PS response is applied to the specimen, which is fixed to the reaction frame. Restoring forces measured from load cells and calculated at constrained DOFs are fed back to the simulation environment that solves the equation of motion. Fig. 5 depicts the constraint setting that was adopted for the substructured wall of our case study.

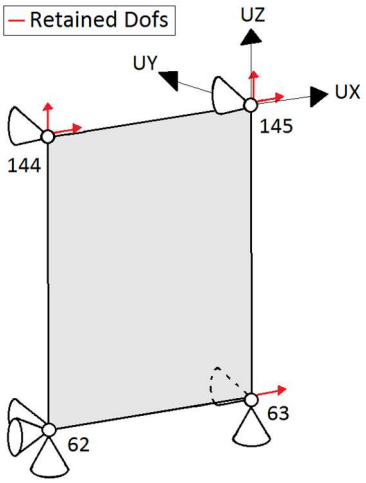

Node	UX	UY	UZ
62	Constrained	Constrained	Constrained
63	Retained	Constrained	Constrained
144	Retained	Constrained	Retained
145	Retained	Constrained	Retained

Figure 5 - Constraint setting for the testing setup of the PS.

As can be appreciated from Fig. 5, seven displacements are constrained while the other five are retained by the experimental setup. According to the current PDT practice, one actuator should handle each retained DOF so as to apply the deformation field to the tested specimen. Arguably, this represents a strong limitation for distributed parameter systems where several experimental DOFs are involved. Bursi and co-workers, [9], recently proposed a method to approximate the PS response with a smaller displacement vector. The basic idea was to optimize actuator placement so as to make specimen deformed configurations spanning the vector space defined by a corresponding reduction basis $\mathbf{T}$ over a reduced number of coordinates $\mathbf{u}^{E*}$,

$$\mathbf{u}^E \approx \mathbf{T}\mathbf{u}^{E*} \tag{8}$$

which allows for condensing PS matrices,

$$\tilde{\mathbf{K}}^P = \mathbf{T}^T \mathbf{K}^P \mathbf{T},\ \tilde{\mathbf{M}}^P = \mathbf{T}^T \mathbf{M}^P \mathbf{T},\ \tilde{\mathbf{f}}^P = \mathbf{T}^T \mathbf{f}^P \tag{9}$$

As a result, given the desired level of approximation, the test can be conducted with the minimum number of actuators. The same approach here is extended to the case of floating PS. In this case, the

reduction basis **T** operates on the sole deformation component of the PS displacement response that is applied to the tested specimen,

$$\bar{\mathbf{u}}^{E,r} \approx \mathbf{T}\bar{\mathbf{u}}^{E_*,r} \tag{10}$$

The following section describes how to formulate this reduction basis.

4.2 Selection of the reduction basis

As anticipated, the effectiveness of the testing setup relies on the optimal selection of the reduction basis **T**. In the following a procedure is proposed that is suitable for automatic implementations and it is scalable up to the desired degree of approximation. It is noteworthy that a robust testing design process should answer the two following questions:

i) Which is the minimum rank of the reduction basis for a given level of approximation?
ii) How to optimize the actuator placement so as to cover the reduction basis span?

Principal Component Analysis (PCA) was proved of valuable help in answering to these questions, [16]. The key idea of PCA is to provide a separated representation of a large number of correlated variables considering a smaller number of uncorrelated variables while preserving the overall process variance, [17]. An orthogonal transformation to the basis of the eigenvectors of the sample covariance matrix is performed, and the data are projected onto the subspace spanned by the eigenvectors corresponding to the largest eigenvalues. This transformation decorrelates the signal components and maximizes the preserved variance. In detail, for any real (m x n) matrix **X** there exists a real factorization called Singular Value Decomposition (SVD) that can be written as,

$$\mathbf{X} = \mathbf{U}\boldsymbol{\Sigma}\mathbf{V}^T \tag{11}$$

where **U** is an (m x m) orthonormal matrix whose columns $\mathbf{u}_i$, namely the left singular vectors, represents the Proper Orthogonal Modes (POMs) while **V** is an (n x n) orthonormal matrix, whose column vectors $\mathbf{v}_i$, namely the right singular vectors, represent the time modulation of the corresponding POMs. **Σ** is an (m x n) pseudo-diagonal and semi-positive definite matrix with singular values σ_i as diagonal entries. From a physical standpoint, singular values relate to the eigenvalues of the autocovariance matrix of the process **X** as,

$$\left\{\sigma_1^2 \quad \ldots \quad \sigma_m^2\right\} = eig\left(\left(\mathbf{X}-\boldsymbol{\mu}_\mathbf{X}\right)\left(\mathbf{X}-\boldsymbol{\mu}_\mathbf{X}\right)^T\right) \tag{12}$$

where $\boldsymbol{\mu}_X$ is a matrix of repeated vectors of time averaged values of **X** . Accordingly, the original data set **X** can be reconstructed up to the desired degree of approximation by retaining a reduced number $q < m$ of POM,

$$\left(\tilde{\mathbf{X}}-\boldsymbol{\mu}_X\right) = \sum_{i=1}^{q}\sigma_i\mathbf{u}_i\mathbf{v}_i^T \tag{13}$$

The most striking property of the Proper Orthogonal Decomposition (POD) is that it minimizes the root mean square error between the original signal **X** and its reduced separated representation $\tilde{\mathbf{X}}$.
In order to show how is possible to use PCA to optimize the design of the testing setup, the time history analysis of the FE model of the drum-dome system subjected to the Loma Prieta earthquake was simulated using the Newmark method, [18], and a data set X was defined on the basis of the deformation response field of the PS,

$$\mathbf{X} = \left[\bar{\mathbf{u}}_1^{E,r} \quad \bar{\mathbf{u}}_2^{E,r} \quad \dots \quad \bar{\mathbf{u}}_n^{E,r} \right] \tag{14}$$

Based on the total data variance $E = \sum_{i=1}^{m} \sigma_i^2$ we defined $E_i = \sigma_i^2 / E$ as the variance fraction carried by the i-th POM. The stem plot of Fig. 6 compares obtained values.

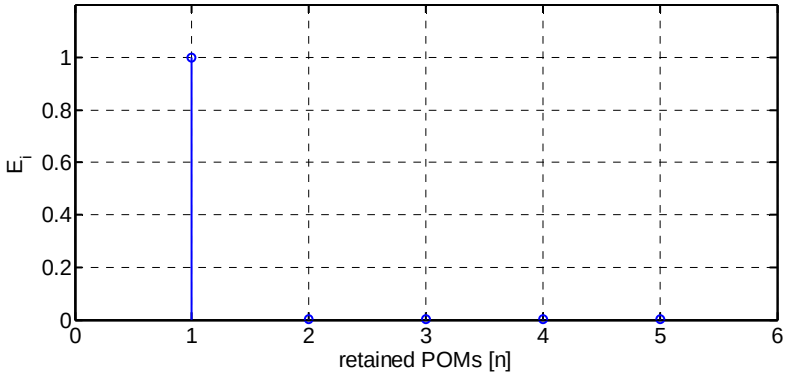

Figure 6 - Fraction of data variance carried by the single POM.

As can be appreciated from Fig. 6, the almost total variance of the deformation component of the displacement response of the PS is carried by the first POM. In order to provide a more physical measure of the degree of approximation of the reconstructed response field, the following Weighted Normalized Root Mean Square Error (WNRMSE) score was introduced,

$$WNRMSE\left(\mathbf{X}, \tilde{\mathbf{X}}\right) = \frac{\sum_{i=1}^{m} NRMSE(\mathbf{x}_i, \tilde{\mathbf{x}}_i) \cdot max\left(\left|\mathbf{x}_i - \boldsymbol{\mu}_{\mathbf{X}_i}\right|\right)}{\sum_{i=1}^{m} max\left(\left|\mathbf{x}_i - \boldsymbol{\mu}_{\mathbf{X}_i}\right|\right)} \tag{15}$$

where,

$$NRMSE(\mathbf{x}, \tilde{\mathbf{x}}) = \frac{\sqrt{\sum_{j=1}^{n} (x_j - \tilde{x}_j)^2 / n}}{|max(\mathbf{x}) - min(\mathbf{x})|} \tag{16}$$

and $\mathbf{x}_i$ represents the time history response of the single i-th retained DOF. As can be argued from Eq. (15) and (16), absolute displacement peaks weight the NRMSE average. Fig. 7 depicts the trend of the WNRMSE up to the total number of POMs.

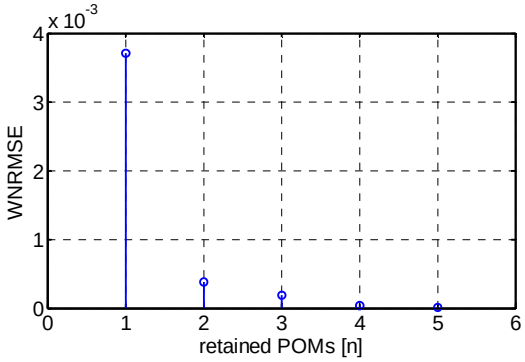

Figure 7 - WNRMSE of the reconstructed deformation component of the PS response

As can be appreciated from Fig. 7, the first POM is arguably sufficient to capture the deformation response of the PS. This is confirmed by Fig. 8 that compares reference and reconstructed signals for DOF 144-X and 145-X, which showed dominant displacement peaks.

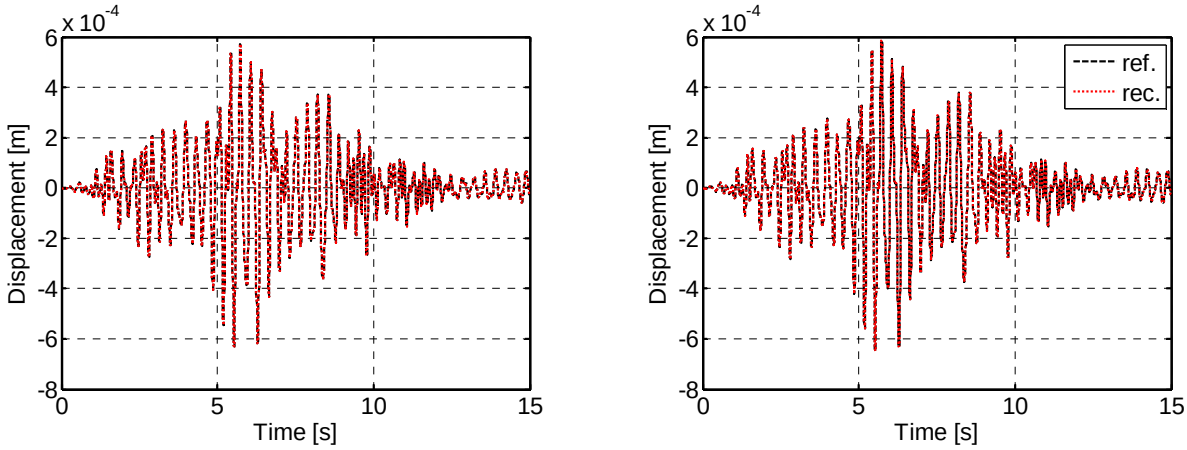

Figure 8 - Reference and reconstructed responses for: a) DOF 144-X; and b) DOF 145-X.

As can be observed from Fig. 8, an almost exact signal reconstruction of the horizontal response is achieved by retaining the first POM only. Analogously, Fig. 9 compare reconstructed signals corresponding to vertical displacements.

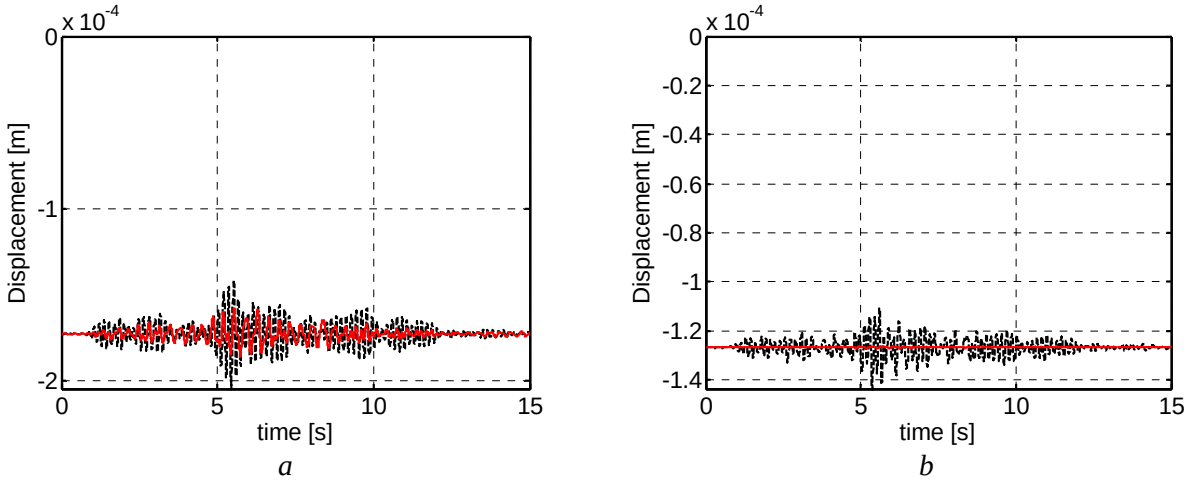

Figure 9 - Reference and reconstructed responses for: a) DOF 144-Z; and b) DOF 145-Z.

As can be appreciated from Fig. 9, the retained POM does not capture the variability of vertical displacements, which is however negligible with respect to average values.

4.3 Actuator placement and validation of the setup

Based on the deformed shape of the retained POM, which is depicted in Fig. 10, the experimental setup layout of Fig. 11 is proposed for testing the PS.

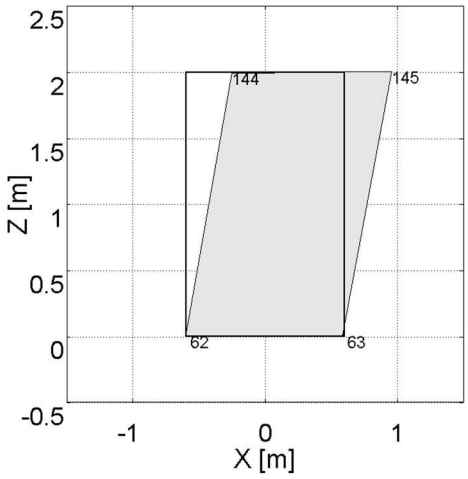

Figure 10 - Retained POM.

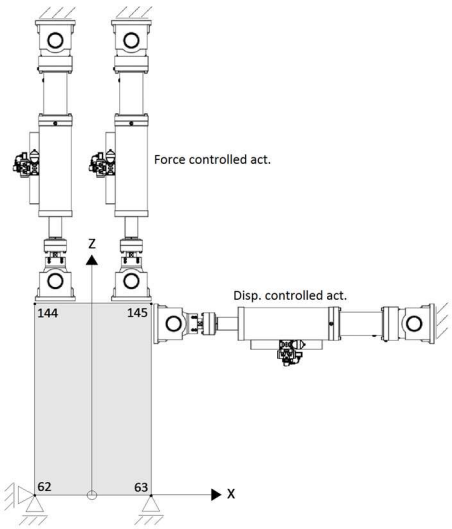

Figure 11 - Experimental setup.

As shown by Fig. 11, the deformed shape of the retained POM indicates a shear deformation of the panel while the variance of the vertical displacements is negligible. Accordingly, a displacement controlled horizontal actuator pushes the top of the wall while two force controlled vertical actuators apply the gravity load coming from the dome. In order to validate the designed testing setup, a reduced order FE model of the drum-dome system was implemented. The reduction basis **T** operating of PS DOFs was obtained by combining deformation modes preserved by the testing setup and rigid body modes, which describe rotations and translations of the floating domain. The Guyan, [19], reduction was applied to obtain the deformation modes $\mathbf{T}_d$ preserved by the setup,

$$\mathbf{T}_d = \begin{bmatrix} \mathbf{I} \\ -\mathbf{K}_{ss}^{P,r^{-1}} \mathbf{K}_{sm}^{P,r} \end{bmatrix} \tag{17}$$

where subscripts *s* and *m* stand for retained slave and master DOF subsets, respectively, and,

$$\mathbf{K}^{P,r} = \begin{bmatrix} \mathbf{K}_{mm}^{P,r} & \mathbf{K}_{ms}^{P,r} \\ \mathbf{K}_{sm}^{P,r} & \mathbf{K}_{ss}^{P,r} \end{bmatrix} \tag{18}$$

is the sub block of the PS stiffness matrix retained by the experimental setup, after discarding DOFs that are physically constrained to the reaction frame. In this case, and according to Fig. 10, master DOFs are DOF 144-X, DOF 144-Z and DOF 145-Z while the slave DOF set includes DOF 145-X and DOF 63-X. It is noteworthy that the Guyan condensation assumes a static deformation of the domain in agreement with the loading procedure of PDT-HS method. Rigid rotations and translations were preserved by retaining corresponding rigid body modes. The resulting reduction basis **T** reads,

$$\mathbf{T} = \begin{bmatrix} \mathbf{T}_d & \mathbf{R}^{P,r} \\ \mathbf{0} & \mathbf{R}^{P,c} \end{bmatrix} \tag{19}$$

Fig. 12 compares the displacement response of DOF 144-X and DOF 144-Z obtained from the reference and the reduced models.

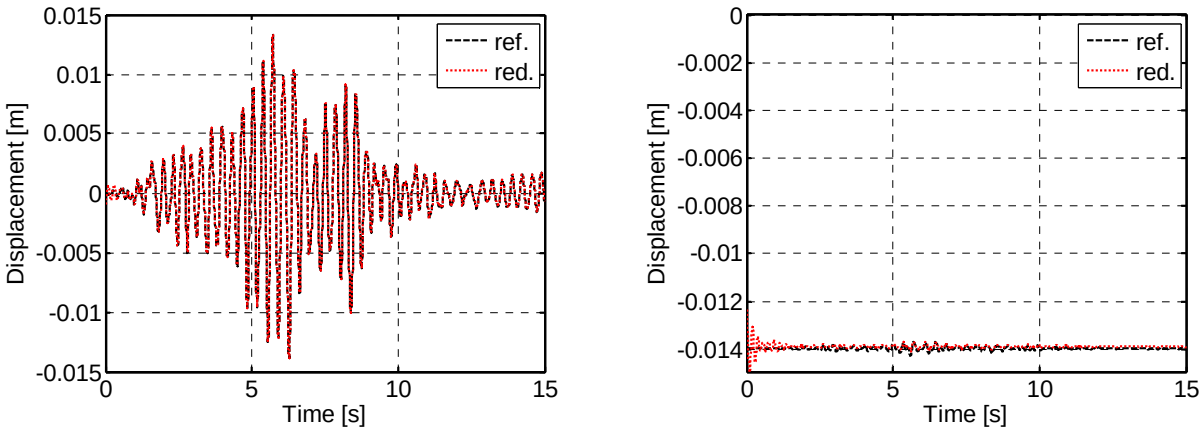

a *b*

Figure 12 - Displacement response of: a) DOF 144-X; and b) DOF 144-Z

As can be appreciated from Fig. 12, the reduced model exactly reproduces the horizontal response obtained from the reference simulation. On the other hand, the small variability of the vertical load justifies the application of a nominal value for testing purpose. Such results corroborate the effectiveness of the test design procedure.

5 CONCLUSION

When simplified structural topologies characterize the physical subdomain, the design of the hybrid simulation testing setup is straightforward. This is not the case when distributed parameters systems are tested in the laboratory and the number of physical degrees-of-freedom tremendously escalates. The concept of reduction basis has been exploited in a previous work to optimize number and position of actuators so as to span the vector space of the expected response of the specimen with the minimum effort. This paper has proposed an effective extension of such study to floating physical subdomain, that is, when the only constraint is provided by the connection to the numerical part of the model. The proposed procedure is suitable for automatic implementations and the numerical validation highlighted its effectiveness. Masonry structures, which are inherently distributed parameter systems, can particularly benefit of the developed approach. A rigorous model-based evaluation of the effectiveness of strengthening interventions is very often impracticable due to the limited knowledge on force redistribution. In this context, hybrid simulation can be profitably used as virtualization paradigm with a potential great impact on cultural heritage conservation.

6 REFERENCES

[1] Takanashi, K., Udagawa, K., Seki, M., Okada, T. & Tanaka, H. Non-linear earthquake response analysis of structures by a computer-actuator on-line system, *Bulletin of Earthquake Resistant Structure Research Center*, Institute of Industrial Science, University of Tokyo, Tokyo, 1975.

[2] Stojadinovic, B., G. Mosqueda, & S. A. Mahin. Event-Driven Control System for Geographically Distributed Hybrid Simulation, *ASCE Journal of Structural Engineering*, Vol. 132, No. 1, pp. 68-77, 2006.

[3] Paquette, J., & Bruneau, M. Pseudo-Dynamic Testing of Unreinforced Masonry Building with Flexible Diaphragm, *M. ASCE2*, DOI: 10.1061/~ASCE!0733-9445~2003!129:6~708!, 2003.

[4] Paquette, J., Bruneau, M. Pseudo-dynamic testing of unreinforced masonry building with flexible diaphragm and comparison with existing procedures, *Construction and Building Materials*, 20, 220–228, 2006.

[5] Pinto, A., Molina, J., Pegon, P., Renda, V. Protection of the cultural heritage at the ELSA Laboratory, ELSA, IPSC, Joint Research Centre, European Commission, I-21020 Ispra (VA) Italy, 2001.

[6] Buonopane, S.G., & White, R.N. Pseudodynamic testing of masonry infilled reinforced concrete frame, *J. Struct. Eng.*, ASCE 125, 578–589, 1999.
[7] Mosalam, K.M., White, R.N., and Ayala, G. Response of infilled frames using pseudo-dynamic experimentation, *Earthquake Engineering and Structural Dynamics*, 27, 589-608, 1998.
[8] Hashemi, M.J., & Mosqueda, G. Innovative substructuring technique for hybrid simulation of multistory buildings through collapse, *Earthquake Engineering and Structural Dynamics*, p. n/a–n/a. doi:10.1002/eqe.2427, 2014.
[9] Bursi O.S. & Wagg D.J. *Modern Testing Techniques for Structural Systems Dynamics and Control.* CISM-Springer, Wien NewYork, 2008.
[10] Aoki Komiyama T., Tanigawa Y., Hatanaka S., Yuasa N., Hamasaki H., Chiorino M.A., Roccati R., Non-Destructive Testing of The Sanctuary of Vicoforte, 13th International Brick And Block Masonry Conference, Amsterdam, 2004.
[11] Calderini C., Chiorino M. A., Roccati R., D'addato C., Aoki T., Spadafora A., Monitoring and Modeling Strategies for the World's Largest Elliptical Dome at Vicoforte, *Structural Analysis of Historical Constructions*, New Delhi, 2006.
[12] Chiorino M.A., Spadafora A., Calderini C., Lagomarsino S., Modeling Strategies for the World's Largest Elliptical Dome at Vicoforte, *International Journal of Architectural Heritage*, Vol.2, P.274-303, 2008.
[13] Chiorino M.A., Ceravolo R., Spadafora A., Zanotti Fragonara L., Abbiati G. Dynamic characterization of complex masonry structures: the Sanctuary of Vicoforte, In: *INTERNATIONAL JOURNAL OF ARCHITECTURAL HERITAGE*, Taylor & Francis, pp 19, pp 296-314, ISSN: 1558-3058, 2011.
[14] Ceravolo, R., Chiorino, M.A., Lai, C., Pecorelli, M.L., Zanotti Fragonara, L. Analysis of long-term monitoring data to assess the efficacy of tie-bars strengthening interventions on a large historical dome, In: SHMII 2015 7th International Conference on Structural Health Monitoring of Intelligent Infrastructure (SHMII 2015), Torino, Italy July 1-3, pp 10, 2015.
[15] ANSYS, ANSYS Academic Research, Release 16.2, 2016.
[16] Bursi O.S., Abbiati G., Reza Md.S. A novel hybrid testing approach for piping systems of industrial plants, *Smart Structures and Systems* 14(6), 1005-1030, DOI: 10.12989/sss.2014.14.6.1005, 2014.
[17] Kerschen, G., Golinval, J., Vakakis, A.F., & Bergman, L. The Method of Proper Orthogonal Decomposition for Dynamical Characterization and Order Reduction of Mechanical Systems: An Overview, *Nonlinear Dynamics*, 41(1-3), 147–169, doi:10.1007/s11071-005-2803-2, 2005.
[18] Newmark, N. M. A method of computation for structural dynamics, *Journal of Engineering Mechanics*, ASCE, 85 (EM3) 67-94, 1959.
[19] Guyan, R.J. Reduction of stiffness and mass matrices, *American Institute of Aeronautics and Astronautics Journal*, 3(2), 380, 1965.